Available online at www.sciencedirect.com
ScienceDirect
Cement and Concrete Research 37 (2007) 1654–1665
Cement and Concrete Research

Microstructural evolution of cemented paste backfill: Mercury intrusion porosimetry test results

Serge Ouellet [a,c,e,*], Bruno Bussière [a,c], Michel Aubertin [b,c], Mostafa Benzaazoua [a,d]

[a] Université du Québec en Abitibi-Témiscamingue, 445, Blvd de l'Université, Rouyn-Noranda, Québec, Canada J9X 5E4
[b] École Polytechnique de Montréal, C.P. 6079, Succ. Centre-Ville, Montréal, Québec, Canada H3C 3A7
[c] Industrial NSERC Polytechnique-UQAT Chair on Environment and Mine Wastes Management, Canada
[d] Canada Research Chair on Integrated Management of Sulphidic Mine Tailings Using Backfill Technology, Canada
[e] GENIVAR, 1462 de la Québécoise, Val-d'Or, Québec, Canada J9P 5H4

Received 7 June 2006; accepted 22 August 2007

Abstract

The microstructural evolution of different cemented paste backfill (CPB) samples made with ground silica was evaluated using mercury intrusion porosimetry (MIP). The influence of three binders (OPC, OPC with fly ash, and OPC with blast furnace slag) and of three types of water (one deionised and two sulphated) on the microstructure was studied over the curing time. Uniaxial compressive strength (UCS) tests were also performed to relate MIP results to the backfill mechanical strength. Among other findings, the MIP analyses indicate that the slag based binder combined with a mixing water having a high sulphate content (of 7549 ppm) showed the highest percentage of fine pores and the highest strength. This behaviour is related to the potential precipitation of sulphate phases in pores, which may contribute to strength enhancement. Based on MIP pore size distributions and UCS results, the authors propose a general relationship applicable for CPB.

Keywords: Cemented paste backfill; Microstructure; Mercury porosimetry; Compressive strength; Mine wastes management

1. Introduction

Mine tailings are generated by ore processing plants and consist of ground rocks from which the valuable minerals have been extracted. The mining industry produces large volumes of tailings that have to be safely managed to avoid significant negative impact to the environment. In modern underground mines, it is a common practice to use an important fraction of the generated tailings as the main component of cemented paste backfill (CPB) material. CPB is usually prepared in surface installations and then transported underground into open stopes via boreholes and pipelines. The material is made by mixing filtered tailings (at a solid content usually between 75 to 85%), binders (3% to7 wt.% of different mix of Portland cement, fly ash, blast furnace slag), and water. The amount of mixing water added is a function of the paste viscosity required to ensure the delivery to underground stopes. CPB provides ground support to the rockmass around mine stopes and allows reducing the amount of tailings sent to surface facilities. Hence the use of CPB may help reducing environmental impacts and capital expenditures related to surface tailings disposal. Surveys conducted over the last few years indicate that CPB is increasingly used as a tailings management option around the world [1,2].

The properties of CPB are similar to those of a controlled low strength material [3]: the water to cement ratio (w/c) is high (usually between 6 and 10); the aggregates used in CPB (tailings) are mainly composed of silt size particles (≈80% <80 μm); and the binder content is usually low at values between 2 to 7% by weight of dry tailings. The CPB strength developed after 92 days is usually between 0.5 to 3 MPa [4–15]. Depending on the ore processed at the mine, tailings can contain sulphide minerals (such as pyrite (FeS_2) and pyrrhotite (FeS)) in proportions that may reach up to 70% [10,13,14,16]. These

* Corresponding author. Tel.: +1 819 825 4274; fax: +1 819 824 1514.
E-mail address: serge.ouellet@genivar.com (S. Ouellet).

0008-8846/$ - see front matter © 2007 Elsevier Ltd. All rights reserved.
doi:10.1016/j.cemconres.2007.08.016

minerals are known to react in the presence of water and oxygen generating acidity, metal hydroxides and sulphate ions [17,18]. These reaction products can affect the behaviour and durability of CPB over the time [7]. Another particularity of CPB is the chemistry of the interstitial water of the paste. Depending on the ore mineralogy and the mineral separation process, this water can contain high concentrations of sulphate and other ions which can affect the hydration process of binders and precipitate in the paste as secondary minerals [7,9,11,19].

In recent years, many papers and reports have been written on CPB characterization and behaviour [8–13,15,20]. Most of these studies relied on a phenomenological approach to develop correlations between mechanical strength and parameter(s) of the CPB recipe. Nevertheless, it is generally accepted in the mining community that a better understanding of the fundamental CPB behaviour would help to optimize CPB preparation and consequently to reduce operating costs.

This paper presents the results of a study on microstructural evolution during the curing of CPB using the mercury intrusion porosimetry (MIP) technique. Other techniques such as scanning electron microscopy (SEM) combined with image analysis and thermogravimetry/differential scanning calorimetry have also been used to study the pore structure and the mineral phases of CPB. However, because of space limitation, the results will not be presented in details here but more information can be found in [21,22]. The main objective of this paper is then to analyse the MIP porosity of CPB during curing and to relate this parameter with the material strength. After a brief overview of MIP tests performed on different geomaterials (cement pastes, natural soils, and CPB), the main results are presented. CPB samples were made from three binders commonly used and three types of mixing water containing typical sulphate concentrations. MIP test results are presented for three curing times: 14, 43 and 92 days. Uniaxial compressive strength (UCS) test results obtained at the same curing times are also presented. An equation relating porosity evolution and mechanical strength is proposed and discussed.

2. Mercury intrusion porosimetry tests performed on CPBs

Mercury intrusion porosimetry (MIP) have been commonly used to evaluate the total porosity and the pore size distribution of different geomaterials. MIP results are usually expressed as the total mercury volume intruded in a sample, giving the MIP total porosity, or by analysing the incremental volume intruded at each pressure step. From the latter representation, Winslow and Diamond [23] named the pore width corresponding to the highest rate of mercury intrusion into the sample the "threshold diameter" (TD). This parameter is important since it can be seen as the smallest diameter of pores that are geometrically continuous throughout the sample. MIP results on cement paste show a decrease of the threshold diameter and of the total porosity with curing time [24,25]. Most MIP tests on cemented materials, such as cement paste and mortar, were performed mainly to define the microstructure evolution during hardening and ultimately to relate microstructural evolution with mechanical strength [26,27].

Over the past few years, some authors have investigated the microstructure of CPB by MIP technique [8,10,15,20,28–30]. Their results show that the CPB total porosity is almost the same as that of tailings only agglomerated with water (between 40 and 45%). Belem et al. [29] also showed that the addition of a mixture of blast furnace slag and Portland cement (80:20) modified tailings pore size distribution. A proportion of 5 wt.% decreased the threshold diameter from 2 to 1 μm approximately. This refinement of the pore size reduces the saturated hydraulic conductivity and increases the water retention properties of the CPB [31]. Fall et al. [20] used MIP to investigate the influence of tailings particle sizes on the microstructure of different CPB mixtures. This study showed that the amount of fine particles (<20 μm) strongly influenced MIP results. The increase in fine particle proportion leads to a decrease in the threshold diameter value (of approximately 1 micron when the proportion of <20 μm particles is increased from 40 to 55%), showing that pore size distribution is also influenced by the grain size distribution of the tailings used in the CPB mixture. Ouellet et al. [30] presented a comparative MIP study between cement pastes (water to cement ratio w/c=0.33) and CPB (w/c=7) samples. Results show that the main mercury intrusion peak was almost two orders of magnitude lower for cement paste samples than for CPB samples. This difference was anticipated due to the high w/c ratio of CPB. According to Powers et al. [32], with a w/c ratio greater than 0.7, capillary pores should never become de-percolated.

To the authors knowledge, no detailed study has been reported on the understanding of the fundamental microstructural evolution of CPB during the curing period, and on the main influence factors affecting porosity and strength.

3. Materials and methods

The present study aims at evaluating the influence of water quality, type and proportion of binder, and curing time on the microstructural evolution of CPBs. The main characteristics of the different materials and methods used are presented in the following.

3.1. Binders

The three binders used in the CPB mixtures are: a 100% type 10 CAN/CSA-A5-98 ordinary Portland cement (named T10 in this study); a mix of 20% T10 and 80% ground granulated blast furnace slag (T10SL); and a mix of 70% T10 and 30% fly ash (T10FA). The Lafarge company provided these binders. The proportions are in the range used in the mining industry to produce CPB [13,14,33]. Fly ash and slag are both by-products of industrial processes. The replacement of a fraction of the Portland cement by these mineral additives in the CPB mixture is often seen as an environmental value-added. Moreover, due to the lower cost of fly ash, its use can significantly reduce overall operational costs of a paste backfill plant [2,30].

The T10 cement shows a typical Bogue's composition of 64.4% for C3 S, 6.6% for C2S, 8.7% for C3A, and 7.4% for C4AF. According to ASTM C618-00 standard, the fly ash can

Table 1
Chemical composition of the waters used in this study (ICP analysis)

	W0	W1	W2
Al (ppm)	0.03	1.06	0.29
Ca (ppm)	0.02	803	1790
Cu (ppm)	<0.01	0.59	0.21
Fe (ppm)	0.05	0.04	1.01
K (ppm)	0.14	41.40	48.00
Mg (ppm)	0.01	1.00	1.71
Na (ppm)	<0.2	915	111
Si (ppm)	3.78	0.82	0.50
Zn (ppm)	<0.02	0.08	0.53
SO_4^{2-} (ppm)	0.36	4613	7549
pH	6.09	9.62	4.57
EhN (mV)	435.8	243.7	361.1
Cond. (μS/cm)	2	5950	3740

be classified as a class C with a cumulative value for SiO_2, Al_2O_3 and Fe_2O_3 of less than 70% and a SO_3 content of less than 5%. Blast furnace slag conforms to ASTM C989-99 and shows the highest BET specific surface among the studied binders with a value of 21 380 cm^2/g. The BET specific surfaces of the other two binder components are 12 764 and 8697 cm^2/g for cement T10 and fly ash respectively.

3.2. Mixing water

CPB mixtures were made with three different types of water: the first one was deionised by filtration (named W0), while the other two mixing waters (named W1 and W2) were sampled at the tailings dewatering process of two mine backfill plants; the latter two contained 4613 ppm and 7549 ppm of SO_4^{2-} respectively. Alkali concentrations are high with 1266 ppm $Na_2O_{eq.}$ and 188 ppm $Na_2O_{eq.}$ for W1 and W2 respectively. One can also see in Table 1 that the calcium content of these waters is relatively high (803 and 1790 ppm for W1 and W2 respectively). Such high concentrations are mainly due to the ore processing techniques at the two mines that use lime to increase the pH. The pH and redox potential (Eh) were measured using the Benchtop pH/ISE Meter Orion model 920A with a coupling of different electrodes. An Orion Triode electrode was used for the pH and the Eh was measured with a Pt/Ag/AgCl combined electrode and then corrected for normal hydrogen electrode (EhN). The pH ranged for the three different waters between 4.57 and 9.62. Waters were filtered to remove suspended particles before analysis and mixing.

3.3. Tailings

For all CPB mixtures ground silica was used to simulate tailings. The silica contains 99.76% SiO_2 and has a grain size distribution (evaluated with a Malvern laser Mastersizer S) close to the average of 11 mine tailings (as sampled from the province of Quebec and Ontario, Canada; see Fig. 1). More than 50% of silica particles are smaller than 25 μm (D_{50}) and 10% smaller than 2 μm (D_{10}). The uniformity coefficient ($C_U = D_{60}/D_{10}$) and the coefficient of curvature ($C_C = D_{30}^2/D_{60} \times D_{10}$) are respectively 16.5 and 1.5. According to the USCS classification [34], the silica material is a non plastic silt (ML), as are most of the tailings produced by hard rock mines [18,35]. Ground silica (a mono-mineral non-reactive aggregate) was selected to focus the study on binder and water chemistry effects on CPB microstructure. Hence, the influence of sulphide (and other) minerals in CPB was not addressed in the present investigation.

3.4. Sample preparation and curing

CPB mixtures were prepared in small batches in a 20-litre bucket and mixed for at least 5 min with a 1/2 inch electric drill using a paint mixer bit. A total of 54 CPB cylinders 10 cm long and 5 cm in diameter were cured at room temperature and at a relative humidity greater than 90%. The binder proportion for the CPB mixtures was 5% by weight of dry silica. Water to cement ratio (w/c) was 7 for all CPB mixtures (representing a water to solid ratio of 0.33); this is representative of values observed in the Canadian mining industry [9,10].

3.5. Drying

The drying method used before MIP tests consisted of a combination of freeze-drying and oven drying. The freeze-drying technique on CPB samples was not able to remove all the free water in a period of 24 h. The authors noticed that freeze-drying was less effective for larger samples and for longer curing period. To accelerate the drying, a second drying period in an oven was introduced as proposed by Kjellsen [36]. More specifically, samples were first cut in small cubes of approximately 1 cm^3 each and immersed for 5 min in liquid nitrogen. They were then dried for a period of 24 h at 0.9 Pascal and −50 °C in a Virtis Ultra 35 Super XL freeze dryer. After the first 24 h, another period of 24 h in an oven at 45 °C completed the drying. This complementary drying stage lead to a constant weight of the CPB samples, which were then maintained in a desiccator to avoid rehydration.

3.6. MIP test procedures

Two cylindrical samples of each mixture were used to evaluate the uniaxial compressive strength (UCS) after 14, 43 and 92 curing days using a MTS 10/GL press with a normal loading capacity of 50 kN and a displacement rate of 0.001 mm/

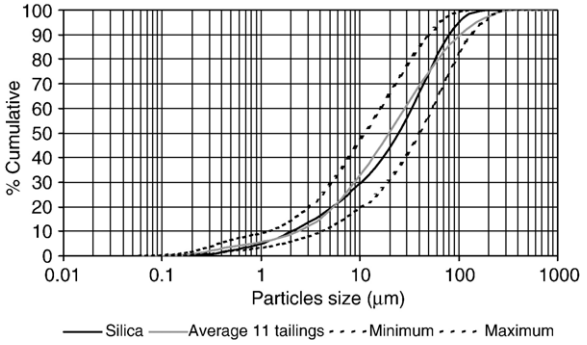

Fig. 1. Volumetric cumulative particles size distribution of silica.

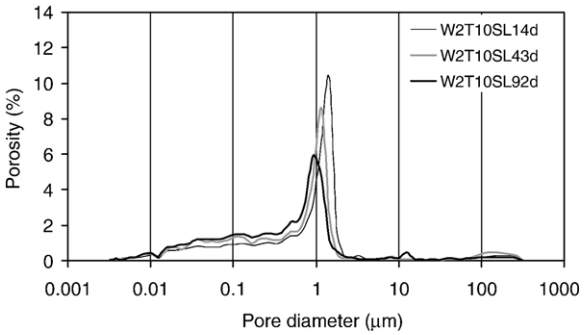

Fig. 2. Pore size distribution of CPB samples W2T10SL at 14, 43, and 92 days.

min. The UCS corresponds to the maximum stress value (failure, peak) reached during the compression test. After the UCS test, the internal part of each cylinder was sampled and dried as described in the previous section. Samples were specifically selected outside the zone affected by the failure plane induced in the cylinders. It can thus be assumed that no significant microstructural damage was induced on the small samples by the strength testing (as microcracks initiation and propagation tend to occur along the main failure plane; see [37]).

MIP tests were performed on CPB samples after each curing period. The equipment used is an Autopore III 9420 from Micromeritics that can generate a maximum pressure of 414 MPa (60 000 psi) and can evaluate a theoretical pore diameter of 0.003 μm. With this machine, the MIP test is performed in two steps: the low pressure step first evacuates gases, fills the sample holder with mercury and performs porosimetry from about 7 to 345 kPa; the high pressure step reaches pressures between 345 kPa and 414 MPa. Low and high pressure steps were always performed within a period of 8 h. The contact angle and surface tension assumed for all tests were respectively 130° and 485 dyn/cm. All tests were performed to achieve the manufacturer recommendation of a mercury stem volume between 25% and 90%. Repeatability of MIP tests was not extensively investigated in this study since the instrument was considered accurate, based on past studies reported in the literature [23,38,39]. However, two repeatability tests (not presented) showed a difference of ±1% on the total MIP porosity, and the mercury intrusion behaviour (pore size distribution) was nearly the same.

3.7. Thermal and chemical analysis

Estimation of sulphate content in samples cured for 92 days was conducted using thermogravimetry/differential scanning calorimetry (TG/DSC) and chemical analysis. TG/DSC tests were performed with the SDT Q600 apparatus from TA Instruments which records simultaneously the weight loss and heat flow during thermal treatment of the sample. Thermal behaviour of samples was registered in an inert nitrogen atmosphere at a rate of 20 °C/min up to 1000 °C. Approximately 35 mg of material, placed in a 90 μl alumina cup and covered by an alumina lid, was used for each test. Previous TG/DSC tests performed on CPB samples indicate that temperature variations between 144–160 °C are associated to gypsum, while and variations between 164–216 °C are associated to monosulphate. The results observed here on CPBs are in the range of those reported for other cement-based materials [40–44].

The selected chemical analysis technique follows the EPA 600/2-78-054 guidelines [45] to determine the sulphate sulphur concentration in each CPB sample. The Sobek method was mainly used to differentiate the sulphate sulphur and the sulphide sulphur in materials containing sulphide oxidation products by selective dissolution in HCl (40% v/v) and in $HNO_3/Br_2/HF$ acids. As the CPB samples did not contain sulphide, only the HCl dissolution was performed and the extracted sulphur amount was assumed to be in precipitated sulphated phases. The resulting solutions were analysed by inductively coupled plasma-atomic emission spectrometry (ICP-AES).

Table 2
MIP porosity (%) and threshold diameter (μm) results

	T10 cement			T10-fly ash cement			T10-slag cement		
	W0	W1	W2	W0	W1	W2	W0	W1	W2
14 days									
Porosity ≥ 0.3 μm	34.92	34.54	36.46	37.25	35.77	34.85	28.51	32.32	31.51
Porosity < 0.3 μm	9.04	10.01	8.54	8.45	8.42	9.84	16.70	12.47	12.94
Total porosity	43.96	44.55	44.99	45.69	44.19	44.69	45.21	44.79	44.46
Threshold diameter	1.42	1.43	1.43	1.44	1.43	1.43	1.17	1.16	1.44
43 days									
Porosity ≥ 0.3 μm	34.36	32.61	33.70	34.53	32.24	33.31	31.86	29.70	27.18
Porosity < 0.3 μm	10.36	10.96	10.13	10.26	11.77	10.35	14.10	14.67	16.77
Total porosity	44.71	43.57	43.83	44.79	44.01	43.65	45.96	44.37	43.94
Threshold diameter	1.17	1.17	1.44	1.44	1.17	1.44	1.17	1.16	1.16
92 days									
Porosity ≥ 0.3 μm	32.30	30.25	31.91	32.74	30.59	31.00	28.51	29.58	26.04
Porosity < 0.3 μm	12.59	14.77	12.50	13.02	13.68	12.61	16.47	14.23	19.06
Total porosity	44.89	45.01	44.41	45.76	44.26	43.60	44.99	43.81	45.11
Threshold diameter	1.17	1.17	1.17	1.17	1.17	1.17	1.16	1.17	0.93

4. MIP porosity results

Fig. 2 presents three MIP pore size distribution curves for the CPB samples W2 T10SL at 14, 43, and 92 days; these results are typical of those measured for the other studied samples. The caption indicates the type of water and binder, and the curing time (e.g. W2 T10SL14d means that this CPB sample was made with W2 water, T10SL binder, and that the UCS test was performed after 14 days of curing). Due to space limitation, all other results are summarized in the Table 2 (all MIP test results can be found in [21]). In the following, the results are analysed with respect to the evolution of these curves, including porosity refinement. In all cases, the MIP tests on CPB show a main intrusion peak at a pressure corresponding to a threshold diameter close to 1.4 μm. This main peak intensity decreases with curing time while there is an increase in the volume of mercury intruded at higher pressure. The mean MIP total porosity for all samples is 44.6% with a standard deviation of 0.66% (see Table 2). Similar porosity results were obtained using a drying technique (at 105 °C) similar to the one frequently used in geotechnical investigations [34] (the porosity is measured using the specific gravity, the dry and humid weight of a given sample having a known volume). The mean porosity values measured with this approach were 45.4%, 45.3%, and 45.4% at 14 days, 43 days, and 92 days respectively; standard deviation for all these porosity values is 0.52%. Hence, there is no significant trend that would point towards a relationship between total porosity, curing time, and binder type.

4.1. Evolution of the threshold diameter

One way to appreciate the effect of curing and of the binder type is to look at the threshold diameter (TD) value (Table 2). In general, there is a pore refinement with curing time. For instance, in the case of the T10 and T10FA samples the TD moves from 1.43 μm at 14 days to 1.17 μm at 92 days. This indicates that as these samples cure, pores tend to become finer because the pressure needed for the mercury to significantly intrude the matrix increases. A somewhat different trend is observed for T10SL. TD values for W0 and W1 waters remain constant at about 1.16 μm for the three curing period studied. Only the mixtures with T10SL and W2 water show a significant curing effect after 43 days; for this sample the TD values drop from 1.44 μm at 14 days to 0.93 μm at 92 days.

4.2. Evolution of the MIP curve

As proposed by few authors [26,27], the analysis of the area under the pore size distribution curve can also be used to represent the pore structure evolution. In the present study, the pore size distribution is divided into two portions: <0.3 μm and ≥ 0.3 μm. According to the definition of the capillary pores [46], pores ≥ 0.3 μm correspond to the main interconnected capillary porosity network. Values given in Table 2 are indicative of a curing effect that is mainly due to a decrease in the TD height with time. The average porosity ≥ 0.3 μm for all samples is 34.0% at 14 days, 32.1% at 43 days, and 30.3% at 92 days. Since the total porosity measured by the MIP tests remains practically unchanged after a curing time of 92 days, this indicated that pores of CPB samples tend to become finer with curing time. The amount of pores ≥ 0.3 μm also shows the effect of the binder type. For all samples at all ages, average porosities are 33.5% for samples using T10 and T10FA binders and 29.4% for samples using T10SL binder. In light of these results, it appears that blast furnace slag seems to generate a finer microstructure in CPB.

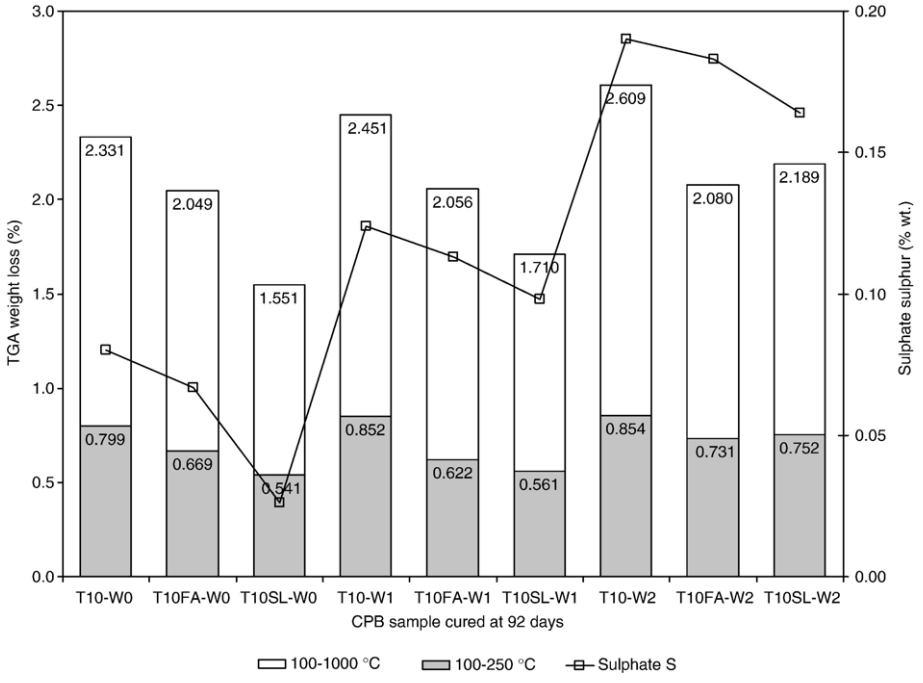

Fig. 3. TGA and chemical analysis results on samples cured at 92 days.

Others have also observed an increase in the proportion of small pores with curing time [25,27]. The evolution of these pores can be related to cement hydration products [25]. This evolution can also be observed on MIP curves reported for CPB [10,20,29], even if it was not specifically noticed by the authors. Table 2 also shows the sum of MIP porosity values for pore sizes less than 0.3 μm. An increase in the relative proportion in this size range is observed with the curing time for all samples except for T10SL using W0 water at 14 days. For all mixtures, the average MIP porosities <0.3 μm are 10.7% at 14 days, 12.1% at 43 days, and 14.3% at 92 days. These results also indicate that the binder T10SL gives the highest proportion of small pores for all curing times. Average porosities <0.3 μm are 11.0%, 10.9%, and 15.3% at all curing times for T10, T10FA, and T10SL binders respectively.

4.3. Influence of mixing water

When samples are sorted by water type, the influence of the water chemistry is not as clear as the binder effect. Average porosity values with a size below 0.3 μm (for all curing times and binder types) are 12.3%, 12.3% and 12.5% for W0, W1 and W2 waters respectively. This slight porosity refinement difference is also accompanied by a slight influence of the water type in the pore fraction ≥0.3 μm; average porosity values are 32.8%, 31.9% and 31.8% for W0, W1 and W2 waters respectively. However, the influence of water quality seems to be more significant for the smaller MIP pore sizes. For instance, when summing MIP porosity values for pore sizes less than 0.1 μm, the average values obtained are 7.2%, 7.5% and 8.2% for W0, W1 and W2 waters respectively.

Hence, for the CPB mixtures made with sulphated water, the precipitation of sulphate minerals in the voids could explain, at least in part, the slight refinement of the pore size. However, as the proportion of cement is low in CPB, spectroscopic mineral determination methods (e.g. XRD or FTIR) are not well adapted to validate this hypothesis. Chemical analysis (Sobek method) and TG/DSC were thus used on samples cured for 92 days to quantify the precipitated sulphated phases in CPB mixtures. TG weight loss results between 100 °C and 250 °C and between 100 °C and 1000 °C are presented in Fig. 3; this figure shows also the measured sulphate sulphur (sulphur in sulphate minerals measured with the Sobek method) concentration in the samples. Based on these, the TG results between 100 °C and 1000 °C can be ranked as T10>T10FA>T10SL; this ranking follows the weight loss order for TG tests performed on unhydrated binders. The TG temperature zone between 100 °C and 250 °C can be related to C–S–H and to sulphates such as ettringite ($Ca_6Al_2(SO_4)3(OH)_{12}\bullet 26H_2O$), gypsum ($Ca(SO_4)\bullet 2H_2O$), and monosulphates (such as $3CaO\bullet Al_2O_3\bullet CaSO_4\bullet 12H_2O$) [41,47]. Except for the T10FA-W0 sample that lost more weight than the T10FA-W1 sample, all other results are in conformity with the hypothesis that more sulphate are precipitated in specimens having more SO_4^{2-} ions in the mixing water. Chemical analysis results are more explicit on the increasing presence of sulphates (in solid form) in samples made with water W1 and W2. Mean concentrations in the CPB samples are 0.06 wt.%, 0.11 wt.% and, 0.18 wt.% for the samples mixed with the waters W0, W1 and, W2 respectively. Additionally, both methods show that amount of precipitated sulphates could be ranked as T10>T10FA>T10SL. This ranking can be explained in part by the lower content in gypsum (contained in ordinary Portland cement) in mixture made of fly ash and slag.

4.4. Influence of the slag

Results previously shown indicate that slag specifically has a different behaviour than the other two binders. It is known that slag has a greater impact on pore refinement in cement pastes than other binders [48,49]; which in turn affects the permeability coefficient [41,50]. The degree of reactivity of the slag particles is proportional to the specific surface, and depends on water availability [51,52]. A particular aspect of slag is its interaction with water: more water is needed for mixture with ordinary Portland cement and slag to achieve the same viscosity [50]. This phenomenon was also observed by Ouellet et al. [30] on cement pastes (w/c=0.33) made with the same binders and waters as the ones used in this study. Mini-slump tests on CPB with W0 water showed slump values of 7.5 cm, 11.5 cm and 5 cm for T10, T10FA and T10SL respectively. Even if CPB is significantly different from concrete or cement paste, results shown here confirm that the particular behaviour of slag observed for cement pastes is also seen with CPB mixtures having a high w/c ratio (w/c fixed to 7 in this study). The degree of reactivity of the slag appears to have a positive (refinement) effect on the pore size distribution of the CPB.

4.5. Influence of MIP test on CPB microstructure

MIP results on CPB show an evolution and a refinement of the pore size over time. It is mainly due to the presence of hydrates and secondary minerals in the CPB matrix. These minerals precipitate in voids, filling them partially or completely [9,11,53]. However, the MIP total porosity (or the volume of mercury that fills the samples) does not change significantly with the curing time. A possible explanation for this phenomenon was proposed by Feldman and Beaudoin [24] and Cook and Hover [25]. Feldman and Beaudoin [24] performed several mercury re-intrusion tests (Hg intrusion followed by a drying step and then re-intrusion on the same sample) on cement pastes and noted that the second intrusion showed coarser MIP pore size distribution and a higher TD value than the first mercury intrusion. These authors raised the possibility that changes occurred in the pore structure during the first intrusion of mercury due to the breakage of pore walls at high pressure. Similar comments were made by Cook and Hover [25] to explain the development of a rounded peak at a diameter of about 0.1 μm in cement pastes. They suggested that mercury crushed hydration products on its path when it filled the sample. According to this hypothesis, the peak developed near 0.1 μm was related to a crushing pressure rather than to the presence of true pores on the MIP distribution curve. Similar experiments to evaluate the influence of the mercury intrusion

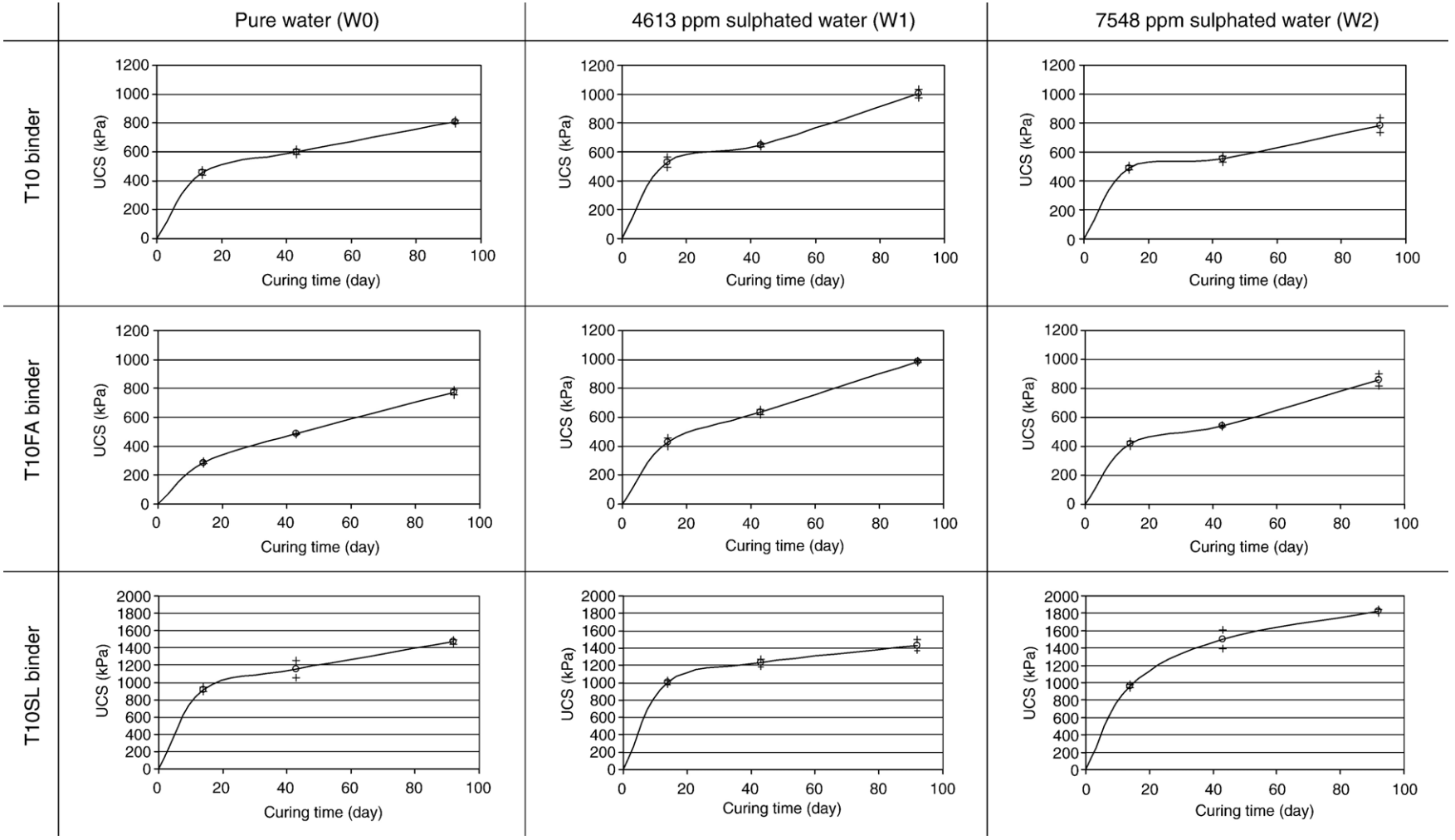

Fig. 4. Mean UCS results for CPB samples; cross marks show minimum and maximum values.

on the microstructure were performed by Lawrence [54] on three fine-grained soils (with a clay fraction ranging from 15 to 60%). Contrary to cement pastes, damages to pore structure by the MIP test were not deemed significant.

To investigate the possible effect of mercury intrusion on the microstructure of CPB samples, mercury re-intrusion tests were performed on two samples. After a first test, samples were dried at 90 °C and 1.5 kPa for 7 days to remove interstitial mercury. Using the differential weight between the sample before the first mercury intrusion and after the drying step, it was inferred that the residual mercury represented approximately 0.002 ml in each sample. 97% of the mercury was then removed from the samples during this phase. The corresponding MIP curves are not presented here (see [21]) but they are quite similar to those shown in Fig. 2. The threshold diameter for all curves is the same (1.16 μm) and the total MIP porosity for the first and the second mercury intrusion are respectively 43.06% and 42.39% for the first sample and 43.05% and 42.02% for the second sample. These differences between the porosity values before and after the re-intrusion test are in the precision range of the MIP technique, estimated at +/− 1%. Therefore, as observed by Lawrence [54] on fine-grained soils, there is no clear evidence of a modification to the internal structure of CPB by the MIP test. The absence of an effect from the mercury intrusion is probably due to the relatively coarse porosity of the CPB, which is offering little resistance to the mercury filling at each pressure step. Samples are thus expected to be completely filled at the end of each test. There is no MIP total porosity decrease observable over the curing time.

5. Relationship between MIP porosity and uniaxial compressive strength

It is generally accepted that the strength of porous materials is a function of the form, quantity, and distribution of the voids [26,55–58]. In general, an increase in total porosity induces a decrease in material strength. Nonetheless, when the voids are filled with precipitated phases, the material strength could be increased by a refinement and segmentation of the porosity and by the different nature of the precipitated phases.

Fig. 4 shows UCS results of the studied CPB samples; these curves show the mean UCS value, with the measured extreme values given as cross marks.

Once again, as for the MIP test results, mixtures using the T10 and the T10FA binders have similar behaviour. For these CPB samples, the UCS ranges from 288 kPa at 14 days to 1004 kPa at 92 days for the three water types. The strength of samples with T10SL binder is higher than that of the other two binders for all samples at all curing times. The highest UCS value measured is 1822 kPa with water W2 at 92 days, which is in accordance with MIP results that showed a finer porosity for this CPB mixture.

Most of physically-based models relating strength and porosity use the total porosity value of the material as the key indicator [56]. As with other engineering materials, the total porosity of cement paste and concrete is typically inversely (and non linearly) proportional to the compressive strength. This dependency is also observed with the MIP porosity. The review of Beaudoin and Marchand [38] presents many relationships between MIP porosity and strength; some of these use the total porosity [59] while others use different portions of the pore size distribution [26,27,60]. In the present study, a strength gain is usually not accompanied by a decrease of the MIP total porosity with time. Nevertheless, the pore size distribution does evolve with curing time, and this change in the microstructure can be related to strength evolution. The following equation is based on a generalized power law expression, which distinguish the contribution of the total porosity and of the size-dependent porosity. Eq. (1). is proposed as a practical means to estimate the strength of CPB samples using the MIP pore size distribution.

$$\sigma_{cn} = \sigma_{n_{min}} \left[\frac{(1-n)}{(1-n_{min})}\right]^{u} \cdot \left[\frac{(1-n_{\geq d})}{(1-n_{<d})}\right]^{V} \quad (1)$$

where σ_{cn} is the compressive strength (UCS) for the CPB having a porosity n; σ_{nmin} is the reference strength at the minimum porosity of the material (n_{min}); n is the MIP total porosity; $n_{\geq d}$ is the cumulative MIP porosity for pores larger than diameter "d" (taken here as 0.3 μm); $n_{<d}$ is the cumulative MIP porosity for pores smaller than diameter "d" (0.3 μm); u and v, are the two exponents that control the non linearity of the two porosity terms on the right hand site of Eq. (1). This relationship can be viewed as an extension of the existing power law functions that relate strength and porosity [55,56,60,61]. Eq. (1) includes two terms to define the porosity dependency: one for the total n value (first bracket on the right hand side of Eq. (1)) and one for the fractional size (second bracket). The minimum porosity value (n_{min}) associated with the maximum strength (σ_{nmin}) of the material is introduced explicitly in Eq. (1) as a reference state. For the materials tested, the minimum porosity n_{min} is estimated at 0.25, based on various test results taken from the literature [62]. For instance, in the case of tailings samples (without binder), Aubertin et al. [63] reported a minimum porosity value of approximately 0.32 at the optimum modified Proctor density, while Mabes et al. [64] reported a value of 0.31 at the end of long term consolidation tests. A minimum porosity value of 0.25 is retained here, considering that an additional porosity reduction (of about 0.06 to 0.07) would appear due to the precipitation of cementitious phases in the CPB [65]. The minimum n value is associated to the maximum strength, which is estimated to be σ_{nmin}=4080 kPa, based on the available results on CPB.

In the proposed equation, the relative contribution of the two fractional size distributions (fine and coarse pore size, based on diameter "d") is used to represent the effect of microstructural evolution. The limiting size "d" (MIP diameter that distinguishes the fine and coarse pore fractions) was fixed at 0.3 μm in this study, based on MIP observations; however, the value of d may be different for other CPBs, as this size-dependency may vary with the material studied. The porosity dependent terms (inside the two brackets of Eq. (1)) are related to strength by a geometric (power law) function, with exponents u and v used to define the non-linearity of the dependency. The value of these

parameters was evaluated with a regression (best fit) analysis, giving: $u=1$ and, $v=5.2$.

Before arriving at Eq. (1), various mechanistic and empirical approaches based on existing formulations were investigated. None of the other expressions were correlated as well to the authors' results, while maintaining a range of application that covers the theoretical value for the porosity variables (which can range from 0 to 1). Eq. (1) includes a term for the total porosity, which is typical of many power law relationships. This term is coupled to a correction factor (second bracket on the right side) that represents the relative contribution of the two fractional porosities. This last term may increase or decrease the uniaxial strength, depending on how the pore size distribution evolves. It can thus be seen as a secondary internal state variable component in the proposed model.

Fig. 5 (a) shows how the total porosity influences the mechanical strength of CPB (represented by the ratio $\sigma_{cn}/\sigma_{nmin}$) for different proportions of fine and coarse pores, expressed from the ratio $(1-n_{\geq 0.3})/(1-n_{<0.3})$. When the latter ratio is fixed, the relationship between $\sigma_{cn}/\sigma_{nmin}$ and the total porosity n appears to be linear (with $u=1$), at least over a certain range (n from 0.25 to 0.60 approximately). Observations on other materials indicate however that the linear dependency may not extend to a larger range of porosity [56], but more data would

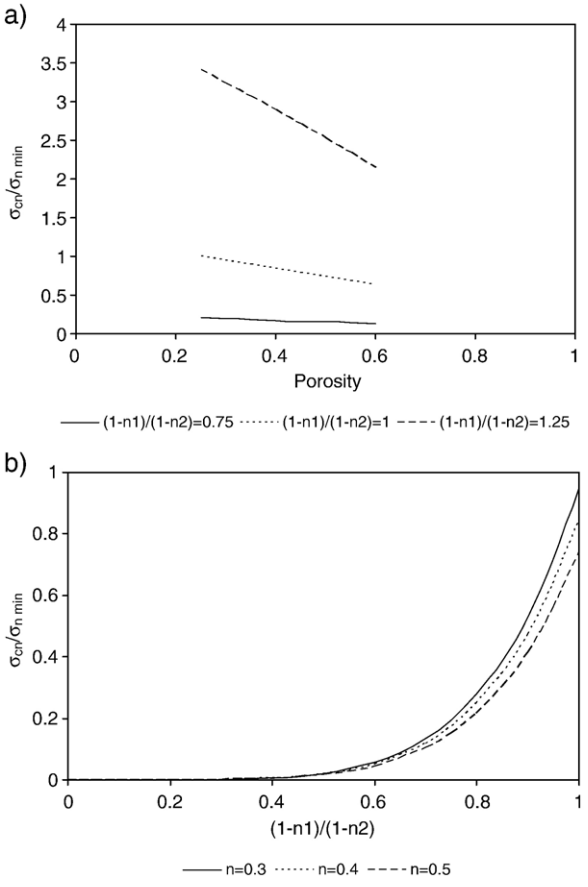

Fig. 5. Graphical representation of Eq. (1) for the relative uniaxial compressive strength: (a) influence of the ratio $(1-n_{\geq 0.3})/(1-n_{<0.3})$ and of the total porosity (for a range between 0.25 and 0.6); (b) influence of the MIP total porosity (in figures: $n1=n_{\geq 0.3}$ and $n2=n_{<0.3}$, i.e. MIP porosity ≥ and <0.3 μm).

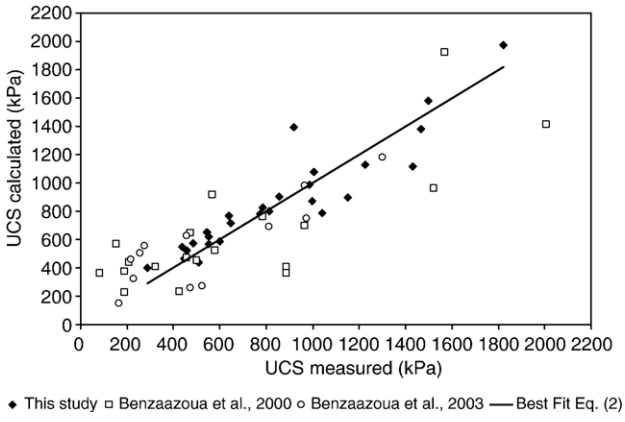

Fig. 6. UCS calculated with Eq. (1) versus UCS measured. Linear fit is applied only on data coming from this study.

be required to evaluate this aspect of the model response. At the same time as the material strength increases when the total porosity decreases, it can also become larger when the ratio $(1-n_{\geq 0.3})/(1-n_{<0.3})$ increases. This is because of a rise in the relative number of small pores (at a fixed porosity) has a positive effect on strength. The contrary applies when the proportion of larger pores is increased. Fig. 5 (b) shows how the ratio of fine to coarse pores influences the material relative strength (i.e. $\sigma_{cn}/\sigma_{n\ min}$) for three typical CPB porosities (0.3, 0.4, and 0.5), according to Eq. (1). As can be seen on this figure, the UCS becomes larger when the ratio $(1-n_{\geq 0.3})/(1-n_{<0.3})$ increases (i.e. with a higher proportion of small pores).

Fig. 6 shows the measured UCS versus the calculated UCS values based on the application of Eq. (1). The coefficient of determination (R^2) between the experimental data presented here and Eq. (1) is relatively high, at 0.83. Higher correlation coefficients could be obtained by including other variables in the model, such as mixture parameters (especially the binder type), but a more global approach is retained here to arrive at a simple relationship based only on porosity terms. Fig. 6 shows some data not included in the database used to develop the model and to perform the initial analysis; these were taken from two independent studies [8,10]. Even if these 31 additional results were obtained with different types of tailings (some samples were made of fine tailings and others with coarser tailings), with another sample preparation procedure, and using different MIP pressure steps; a similar trend between MIP porosity and strength is observed. The coefficient of determination (R^2) between measured UCS and calculated UCS for all points included in Fig. 6 is 0.66 when forcing the linear regression to go through the origin (i.e. 0,0 coordinates). Considering the numerous influence factors involved in the mixing, testing, and basic nature of the various CPB, this tend to indicate that the same trend would apply to various types of CPB. Of course, additional data are required to confirm this preliminary assumption.

As *in situ* sampling is expensive, Eq. (1) could provide a useful means to estimate the strength of CPB when only small pieces of material are available. After a few tests, this relationship could also be calibrated on a given site to provide

the variations of CPB strength in a mine where the conditions are expected to vary from one stope to the other (and even within a given stope). However, more work will have to be performed to validate the proposed equation for a wider range of conditions, including different types of CPB. It is worth emphasizing that the proposed estimation method does not eliminate the need for a detailed mechanical characterization of CPB samples with traditional approaches (UCS and triaxial tests).

6. Summary and conclusion

Microstructural evolution of different cement paste backfill (CPB) samples made with ground silica was measured by mercury intrusion porosimetry (MIP). Three binders were used at 5% by weight of dry silica: a type 10 Portland cement alone (T10), a mix 20:80 of T10 and blast furnace slag (T10SL) and a mix 70:30 of T10 and fly ash (T10FA). Three different types of water were used in the preparation of the mixtures: a deionised water and two waters sampled from two mine backfill plants and containing 4613 and 7549 ppm $SO4^{2-}$. These waters are representative of a true interstitial water of highly sulphidic tailings. Uniaxial compressive strength (UCS) tests were also performed on the different CPB mixtures to investigate the link between pore size distribution and mechanical strength. Based on the results obtained, the following conclusions can be drawn:

1. MIP test is sufficiently sensitive to detect differences between porosity evolutions of different CPB mixtures containing 5% by weight of binder.
2. The threshold diameter (TD) decreases with curing time for all mixtures, indicating a decrease in pore size in the main pore network. The quantity of pores below the main intrusion peak increases with curing time for all mixtures, showing a porosity refinement due to the hydration process.
3. For the curing period and for the types of water used, the CPB samples made with sulphated waters usually showed a higher UCS value, with a smaller TD size. There was also a slight increase in the relative proportion of smaller pores. Precipitation of sulphated minerals in voids could explain this observation.
4. CPB samples made of binder T10SL showed the highest percentage of fine pores and the highest UCS values. The fineness of the slag particles induced a more effective water to binder cementitious effect than that of the other two binders studied.
5. CPB mixtures with fly ash showed a similar pore size distribution and strength evolution as CPB mixtures with ordinary Portland cement (OPC) alone. Since fly ash is cheaper than OPC and it contributes to reduce CO_2 emission, a partial replacement (30%) in the CPB mixture can be seen as an environmental and economical opportunity.
6. For all samples at all curing times, MIP total porosity remained at approximately 44%. Mercury re-intrusion tests performed on CPB samples showed that the test did not significantly affect the internal structure of the material. This would indicate that because of the high w/c ratio and the low binder percentages, the hydration/precipitation phenomena do not significantly affect the total porosity of CPB.
7. In spite of a constant MIP total porosity, the MIP pore size distribution is affected by different factors such as curing time, binder type and proportion, and, to a smaller extent, water quality. The pore size distribution curve of CPB samples was divided into two fractional sizes (<0.3 μm; ≥ 00.3 μm), and these were related to the UCS evolution. A simple equation is proposed to represent the pore-size dependency of the strength.

CPB is a particular material that has a unique evolutive microstructure. This study has led to a better understanding of the influence of some important factors, including binder type, curing time, and water quality, on the microstructural evolution of CPB. The authors were also able to correlate this evolution with the mechanical strength of the material. Despite the promising results, more work is needed to evaluate other types of CPB and to assess the influence of other parameters on CPB microstructure. In this regard, work is ongoing to study the effect cement proportion, tailings grain size distribution and mineralogy.

Acknowledgments

Funding of this work came from the Industrial NSERC Polytechnique-UQAT Chair on Environment and Mine Wastes Management (http://www.polymtl.ca/enviro-geremi). An NSERC Postgraduate Scholarship to the first author also supported this research. Finally, the first author would like to thank colleagues at URSTM for their support, and Professor Tikou Belem for his valuable comments on MIP results.

References

[1] E. De Souza, D. DeGagné, J.F. Archibald, Minefill applications, practices and trends in Canadian mines, Proceedings of the 7th International Symposium on Mining with Backfill, Society for Mining, Metallurgy, and Exploration, 2001, pp. 311–319.
[2] M. Benzaazoua, D. Bois, T. Belem, P. Gauthier, S. Ouellet, M. Fall, J.F. St-Onge, Remblais souterrains, évolution des connaissances et de la pratique, in: 20th Colloque Contrôle de terrains, Association Minière du Québec, Val d'Or, Quebec, Canada, 2005, 23 p.
[3] Aci Committee 229, Controlled Low-strength Materials (CLSM), ACI, vol. 229R-299, American Concrete Institute, 1999.
[4] L. Liping, Solidification and strengthening of mine tailings using a high-water rapid-setting cement, Master Thesis, Technical University of Nova-Scotia, Halifax, Canada, 1997.
[5] A. Grice, Underground mining with backfill, The 2nd Annual Summit – Mine Tailings Disposal Systems, Brisbane, Australia, 1998, 6 p.
[6] A.B. Annor, A study of the characteristics and behaviour of composite backfill material, Ph. D. Thesis, McGill University, Montreal, Canada, 1999.
[7] M. Benzaazoua, J. Ouellet, S. Servant, P. Newman, R. Verburg, Cementitious backfill with high sulfur content: physical, chemical and mineralogical characterization, Cem. Concr. Res. 29 (5) (1999) 719–725.
[8] M. Benzaazoua, T. Belem, D. Jolette, Investigation de la stabilité chimique et son impact sur la qualité des remblais miniers cimentés, IRSST Report R-260, ISBN: 2-551-20431-3, 2000.

[9] M. Benzaazoua, T. Belem, B. Bussière, Chemical factors that influence the performance of mine sulphidic paste backfill, Cem. Concr. Res. 32 (7) (2002) 1133–1144.
[10] M. Benzaazoua, M. Fall, S. Ouellet, Étude pluridisciplinaire visant à mettre au point un outil expert pour la prédiction du comportement des remblais en pâte, IRSST Research Project 099–085, Final Report, 2003, 187 p.
[11] M. Benzaazoua, M. Fall, T. Belem, A contribution to understanding the hardening process of cemented pastefill, Miner. Eng. 17 (2) (2004) 141–152.
[12] A. Kesimal, B. Ercikdi, E. Yilmaz, The effect of desliming by sedimentation on paste backfill performance, Miner. Eng. 16 (10) (2003) 1009–1011.
[13] A. Kesimal, E. Yilmaz, B. Ercikdi, Evaluation of paste backfill mixtures consisting of sulphide-rich mill tailings and varying cement contents, Cem. Concr. Res. 34 (10) (2004) 1817–1822.
[14] J. Cayouette, Optimization of the paste backfill plant at Louvicourt mine, CIM Bull. (Nov/Dec 2003) 51–57.
[15] K.-A. le Roux, In situ properties and liquefaction potential of cemented paste backfill, Ph. D. thesis, University of Toronto, Canada, 2004.
[16] C. Goulet, S. Blais, Utilisation du remblai en pâte à la mine Bouchard-Hébert, in: 16e Colloque en contrôle de terrain, Association minière du Québec, Val d'Or, Québec, Canada, 2001, 21 p.
[17] V.P. Evangelou, Pyrite Oxidation and Its Control, CRC Press, 1995.
[18] M. Aubertin, B. Bussière, L. Bernier, Environnement et gestion des rejets miniers, Manual on CD-ROM, Presses Internationales Polytechnique, 2002.
[19] J.C. Subauste, I. Odler, Stresses generated in expansive reactions of cementitious systems, Cem. Concr. Res. 32 (1) (2002) 117–122.
[20] M. Fall, M. Benzaazoua, S. Ouellet, Experimental characterization of the influence of tailings fineness and density on the quality of cemented paste backfill, Miner. Eng. 18 (1) (2005) 41–44.
[21] S. Ouellet, Mineralogical characterization, microstructural evolution and environmental behaviour of mine sulphidic cemented paste backfills, Ph. D. Thesis, Université du Quebec en Abitibi-Témiscamingue, Canada, 2006, (http://www.uqat.ca/bibliotheque/theses/sergeouellet.pdf).
[22] S. Ouellet, B. Bussière, M. Benzaazoua, M. Aubertin, SEM-XMAP: Scanning Electron Microscopy and X-Ray Dot-Mapping Applied to Cemented Paste Backfill, Proceedings of CIM MineFill2007 Conference, Montreal, Canada, 2007, 10 p.
[23] D.N. Winslow, S. Diamond, A mercury porosimetry study of the evolution of porosity in portland cement, J. Mater. 5 (3) (1970) 564–585.
[24] R.F. Feldman, J.J. Beaudoin, Pretreatment of hardened hydrated cement pastes for mercury intrusion measurements, Cem. Concr. Res. 21 (2–3) (1991) 297–308.
[25] R.A. Cook, K.C. Hover, Mercury porosimetry of hardened cement pastes, Cem. Concr. Res. 29 (6) (1999) 933–943.
[26] M. O'Farrell, S. Wild, B.B. Sabir, Pore size distribution and compressive strength of waste clay brick mortar, Cem. Concr. Compos. 23 (2001) 81–91.
[27] L. Jiang, Y. Guan, Pore structure and its effect on strength of high-volume fly ash paste, Cem. Concr. Res. 29 (4) (1999) 631–633.
[28] M. Benzaazoua, Caractérisation physico-chimique et minéralogique de produits miniers sulfurés en vue de la réduction de leur toxicité et de leur valorisation. Ph. D. Thesis, Institut National Polytechnique de Lorraine, Nancy, France, 1996.
[29] T. Belem, B. Bussière, M. Benzaazoua, The effect of microstructural evolution on the physical properties of paste backfill, Proceedings of Tailings and Mine Waste'01, Balkema, Rotterdam, ISBN: 90 5809 182 1, 2001, pp. 365–374.
[30] S. Ouellet, B. Bussière, M. Benzaazoua, M. Aubertin, T. Belem, Effect of binder type and mixing water chemistry on microstructural evolution of cemented paste backfill, Proceedings of the 57th Annual Canadian Geotechnical Conference and 5th joint IAH-CNC/CGS Conference, Quebec, Canada, 2004, 8 p.
[31] J. Godbout, Évolution des propriétés hydriques des remblais miniers cimentés en pâte durant le curage, M. Sc. A. Thesis, École Polytechnique de Montréal, Montréal, Canada, 2005.
[32] T.C. Powers, L.E. Copeland, H.M. Mann, Capillary continuity or discontinuity in cement pastes, J. Port. Cem. Assoc. Res. Dev. Lab. 1 (2) (1959) 38–48.
[33] T. Grice, Recent minefill developments in Australia, Proceedings of the 7th international symposium on mining with backfill, Seattle, Washington, 2001, 5 p.
[34] D.F. McCarthy, Essentials of Soil Mechanics and Foundations, Prentice Hall, 2002.
[35] S.G. Vick, Planning, Design, and Analysis of Tailings Dams, Bitech, Vancouver, 1990.
[36] K.O. Kjellsen, Heat curing and post-heat curing regimes of high-performance concrete: Influence on microstructure and C–S–H composition, Cem. Concr. Res. 26 (2) (1996) 295–307.
[37] D.P. Sainsbury, R. Urie, Stability analysis of horizontal and vertical paste fill exposures at the Raleigh Mine, Proceedings of CIM MineFill2007 Conference, Montreal, Canada, 2007, 9 p.
[38] J.J. Beaudoin, J. Marchand, Pore Structure, in: V.S. Ramachandran, J.J. Beaudoin (Eds.), Handbook of Analytical Techniques in Concrete Science And Technology, National Research Council of Canada, Noyes Publications, 2001, pp. 528–628.
[39] P.H. Simms, E.K. Yanful, A discussion of the application of mercury intrusion porosimetry for the investigation of soils, including an evaluation of its use to estimate volume change in compacted clayey soils, Géotechnique 54 (6) (2004) 421–426.
[40] I. Odler, S. Abdul-Maula, Possibilities of quantitative determination of the AFt-(ettringite) and AFm-(monosulphate) phases in hydrated cement pastes, Cem. Concr. Res. 14 (1) (1984) 133–141.
[41] H.F.W. Taylor, Cement Chemistry, Academic Press, New York, 1990.
[42] K. Kovler, Setting and hardening of gypsum–portland cement–silica fume blends, Part 2: early Strength, DTA, XRD, and SEM Observations, Cem. Concr. Res. 28 (4) (1998) 523–531.
[43] Q. Zhou, F.P. Glasser, Thermal stability and decomposition mechanisms of ettringite at <120 °C, Cem. Concr. Res. 31 (9) (2001) 1333–1339.
[44] V.S. Ramachandran, R.M. Paroli, J.J. Beaudoin, A.H. Delgado, Handbook of thermal analysis of construction material, Noyes Publication, William Andrew Publishing, 2002.
[45] A.A. Sobek, W.A. Schuller, J.R. Freeman, R.M. Smith, Field and laboratory methods applicable to overburden and minesoils, EPA 600/2–78–054, 1978.
[46] T.C. Powers, The physical structure and engineering properties of concrete, Res. Dev. Lab. Portland Cement Assoc. 90 (1958) 28 p.
[47] V.S. Ramachandran, J.J. Beaudoin, Handbook of Analytical Techniques in Concrete Science and Technology, National Research Council of Canada, Noyes Publications, 2001.
[48] R. Luo, Y. Cai, C. Wang, X. Huang, Study of chloride binding and diffusion in GGBS concrete, Cem. Concr. Res. 33 (1) (2003) 1–7.
[49] Q. Niu, N. Feng, J. Yang, X. Zheng, Effect of superfine slag powder on cement properties, Cem. Concr. Res. 32 (4) (2002) 615–621.
[50] V.M. Malhotra, High performance, high volume fly ash concrete for sustainability, in: A. Tagnit-Hamou, K.H. Khayat, R. Gagné (Eds.), P.-C. Aïtcin Symposium on the Evolution of Concrete Technology, American Concrete Institute, Quebec and Eastern Ontario Chapter, Canada, 2001, pp. 19–74.
[51] J.I. Escalante, L.Y. Gomez, K.K. Johal, G. Mendoza, H. Mancha, J. Mendez, Reactivity of blast-furnace slag in Portland cement blends hydrated under different conditions, Cem. Concr. Res. 31 (10) (2001) 1403–1409.
[52] J.S. Lumley, R.S. Gollop, G.K. Moir, H.F.W. Taylor, Degrees of reaction of slag in some blends with Portland cements, Cem. Concr. Res. 26 (1) (1996) 139–151.
[53] M. Fall, M. Benzaazoua, Modeling the effect of sulphate on strength development of paste backfill and binder mixture optimization, Cem. Concr. Res. 35 (2) (2005) 301–314.
[54] G.P. Lawrence, Stability of soil pores during mercury intrusion porosimetry, J. Soil Sci. 29 (1978) 299–304.
[55] A.M. Neville, Properties of concrete, Longman Scientific & Technical, 1981.
[56] L. Li, M. Aubertin, A general relationship between porosity and uniaxial strength of engineering materials, Can. J. Civ. Eng. 30 (4) (2003) 644–658.
[57] R. Bahar, M. Benazzoug, S. Kenai, Performance of compacted cement-stabilised soil, Cem. Concr. Compos. 26 (2004) 811–820.

[58] A. Katz, K. Kovler, Utilization of industrial by-products for the production of controlled low strength materials (CLSM), Waste Manag. 24 (2004) 501–512.
[59] C.S. Poon, Y.L. Wong, L. Lam, The influence of different curing conditions on the pore structure and related properties of fly-ash cement pastes and mortars, Constr. Build. Mater. 11 (7–8) (1997) 383–393.
[60] I. Odler, M. Röbler, Investigations on the relationship between porosity, structure and strength of hydrated Portland cement pastes. II. Effect of pore structure and of degree of hydration, Cem. Concr. Res. 15 (3) (1985) 401–410.
[61] V. Rzhevsky, G. Novik, The physics of rocks, MIR Publisher, Moscow, 1971.
[62] B. Bussière, Évaluation des propriétés hydrogéologiques des résidus miniers utilisés comme barrières de recouvrement, M. Sc. A. Thesis, École Polytechnique de Montréal, Montréal, Canada, 1993.
[63] M. Aubertin, B. Bussière, R.P. Chapuis, Hydraulic conductivity of homogenized tailings from hard rock mines, Can. Geotech. J. 33 (1996) 470–482.
[64] D.L. Mabes, H.H. James, R.E. Williams, Physical properties of Pb–Zn mine-process wastes, Proceedings of Conference on Geotechnical Practice for Disposal of Solid Waste Materials, American Society of Civil Engineers, 1977, pp. 103–117.
[65] S. Ouellet, B. Bussière, M. Mbonimpa, M. Benzaazoua, M. Aubertin, Reactivity of an underground mine sulphidic cemented paste backfill, Miner. Eng. 19 (2006) 407–419.